Journal of Hazardous Materials 169 (2009) 626–634

Contents lists available at ScienceDirect

Journal of Hazardous Materials

journal homepage: www.elsevier.com/locate/jhazmat

Effect of Al_2O_3 mole fraction and cooling method on vitrification of an artificial hazardous material. Part 1: Variation of crystalline phases and slag structures

Yi-Ming Kuo [a,*], Kuo-Lin Huang [b], Chih-Ta Wang [a], Jian-Wen Wang [a]

[a] Department of Safety Health and Environmental Engineering, Chung Hwa University of Medical Technology, Tainan County, 71703, Taiwan, ROC
[b] Department of Environmental Engineering and Science, National Pingtung University of Science and Technology, Ping Tung 91201, Taiwan, ROC

ARTICLE INFO

Article history:
Received 21 November 2008
Received in revised form 13 March 2009
Accepted 4 April 2009
Available online 14 April 2009

Keywords:
Al ion
Amorphous
Vitrification
Slag
Crystalline phase

ABSTRACT

This study investigated how Al ions affect slag structure. During vitrification, pure Al_2O_3, CaO, and SiO_2 served as the encapsulation phases with the use of Al mol% as an operating parameter. All specimens with the same basicity (mass ratio of CaO to SiO_2) of 2/3 were vitrified at 1400 °C and cooled by air cooling or water quenching. XRD was used to measure the volume fractions of crystalline and amorphous phases. In a non-Al environment, $CaSiO_3$ was formed in air-cooled and water-quenched slags. With the addition of Al_2O_3, no crystalline phases were observed in water-quenched slags. With the increase of Al mol% in specimens, the Al ions in air-cooled slags initially acted as an intermediate linking one tetrahedron chain to another and reducing the amount of crystalline phase, then behaved as a network former making the slags amorphous, and finally replaced Si ions in silicate frames to generate a large amount of $CaAl_2Si_2O_8$. Air cooling improved the formation of crystallize structures with more leachable metal ions. A highly crystallized Al-framed structure is not suitable for encapsulating hazardous metals in vitrified slags.

1. Introduction

Vitrification is widely used to treat hazardous materials such as fly ashes, electroplating sludge, and nuclear wastes [1–3], because it may be applied to destroy organic toxics, recover metals, and stabilize hazardous metals [4–6]. Slags obtained from vitrification are commonly reused as additives for building materials, glassy ceramics, or cements [7,8]. For such cases, the immobilization of hazardous metals is especially important from an environmental point of view. To vitrify the wastes containing toxic metals, the ternary glass matrix system of $CaO–Al_2O_3–SiO_2$ (CAS) plays an important role in encapsulating hazardous metals. The mass ratio of CaO to SiO_2 in an original specimen is defined as its basicity, which is usually adopted to evaluate the control of vitrification processes. In a glass matrix, the most important components for glass networks are Si and O, and these two basic elements often influence the slag structure. Ca ions also affect the slag structure because they randomly distribute through the structure to provide local charge sites, and therefore, they act as network modifiers to modify the network structure. For years, many studies have been conducted to explore how basicity governs vitrification processes [9,10].

In addition to Si and Ca cations, Al^{3+} also plays an important role in the formation of crystalline structures because it acts as both a network modifier and an intermediate in silicate minerals [11]. However, little attention has been paid to the effect of Al_2O_3 on the structures of slags or the immobilization of hazardous metals.

In a random glass network model, the coordination number of O ions of SiO_4 tetrahedra and $(AlO_4)^-$ tetrahedra is 4. The Si and Al ions are both network formers. However, Al ions, with a coordination number of 6, may link tetrahedral silicate groupings through a simple ionic bond and are thus referred to as intermediates [12].

A few researchers have investigated how Al_2O_3 addition affects physical properties of slags. One study reported that increasing the amount of Al_2O_3 enhanced early hydration of cement but excessive amounts of Al_2O_3 decreased strength of a slag when the slag was blended with Portland cement [13]. The amount of Al_2O_3 greatly affects the crystallization of slags in a CAS system [14]. Al_2O_3 governs the structure of a slag and is significantly associated with strength of the slag, but little is known about how Al_2O_3 influences the immobilization of hazardous materials. When recycling slags vitrified from hazardous materials, encapsulation is more important than physical properties. Therefore, we explored the effect of Al ions and two cooling ways on the crystalline characteristics of slags and the encapsulation of metals. The results are provided by two sections: Part 1: variation of crystalline phases and slag structures, and Part 2: encapsulation of metals and resistance to acid. The former, presented in this paper, discussed the volume fractions of crystalline phases and amorphous phases of slags. The influences of Al_2O_3 mole fraction and the cooling method on the formation of slag structures were also investigated. The microstructures of slags

* Corresponding author. Tel.: +886 6 2674567x854; fax: +886 6 2675049.
E-mail address: yiming@mail.hwai.edu.tw (Y.-M. Kuo).

0304-3894/$ – see front matter © 2009 Elsevier B.V. All rights reserved.
doi:10.1016/j.jhazmat.2009.04.015

Table 1
Physical properties of targeted metals.

Targeted metal	Boiling point (°C)	Specific weight
Cr	2200	7.1
Cu	2300	8.9
Mn	1900	7.2
Ni	2900	8.9
Pb	1620	11.3

Table 2
Composition in mol% of the glass matrix of the original specimens.

Specimen (%)	Al_2O_3 (as Al ions)	CaO (as Ca ions)	SiO_2 (as Si ions)
A-0, W-0	0.0	41.7	58.3
A-1, W-1	5.7	39.3	55.0
A-2, W-2	11.3	37.0	51.8
A-3, W-3	16.8	34.7	48.5
A-4, W-4	22.2	32.4	45.4
A-5, W-5	27.6	30.2	42.2
A-6, W-6	32.9	28.0	39.1

Table 3
Compositions and percent mass retained (PMR) data of slags.

	A-0				W-0			
Targeted metal	Range (mg/kg)	Average (mg/kg)	RSD (%)	PMR	Range (mg/kg)	Average (mg/kg)	RSD (%)	PMR
Cr	1220–1260	1240	1.90	1.23	969–1070	1020	5.12	1.23
Cu	767–902	855	8.91	0.847	451–563	517	11.4	0.512
Mn	1410–1530	1450	4.50	1.44	1170–1370	1270	7.71	1.26
Ni	1020–1250	1130	9.87	1.12	726–854	809	8.88	0.801
Pb	176–181	178	3.30	0.176	193–200	197	2.80	0.199

RSD: relative standard deviation(= standard deviation/average × 100%).

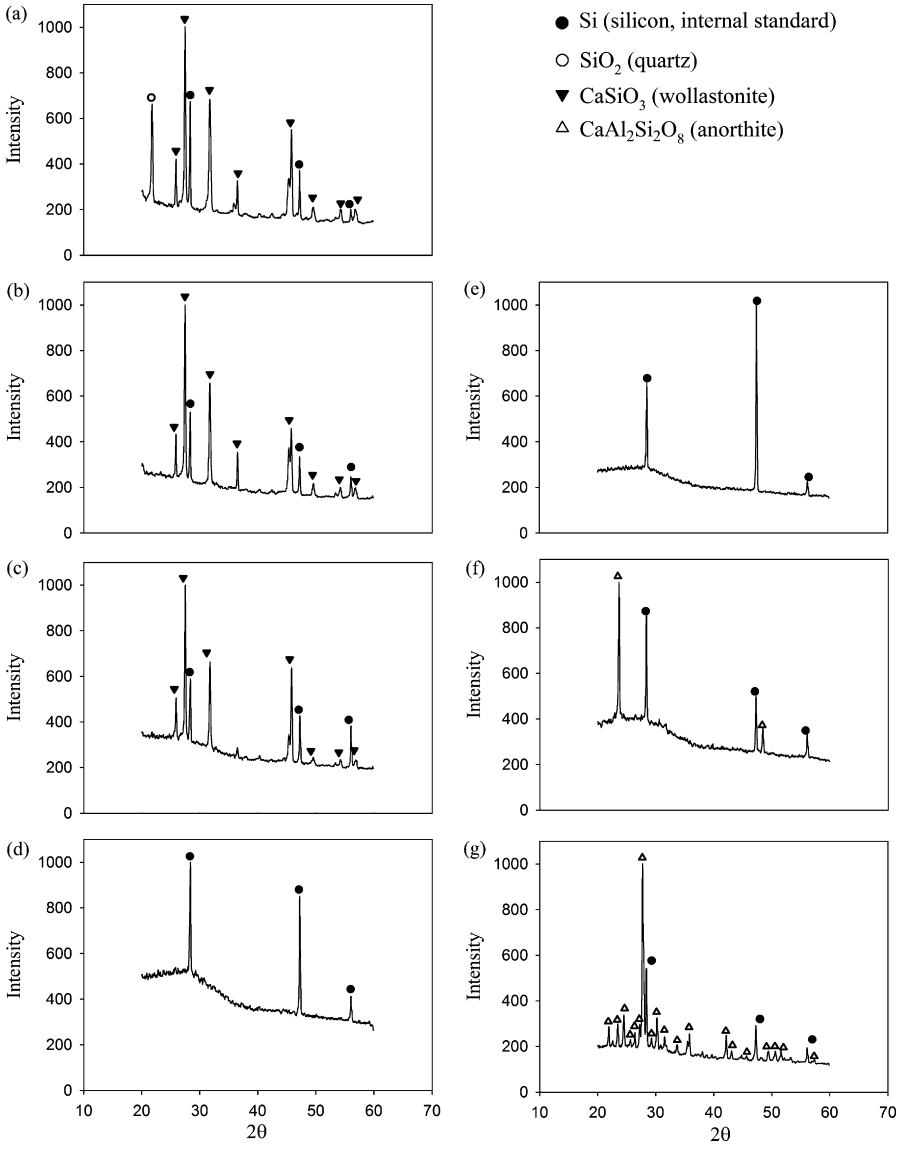

Fig. 1. XRD patterns of air-cooled slags: (a) A-0, (b) A-1, (c) A-2, (d) A-3, (e) A-4, (f) A-5, and (g) A-6.

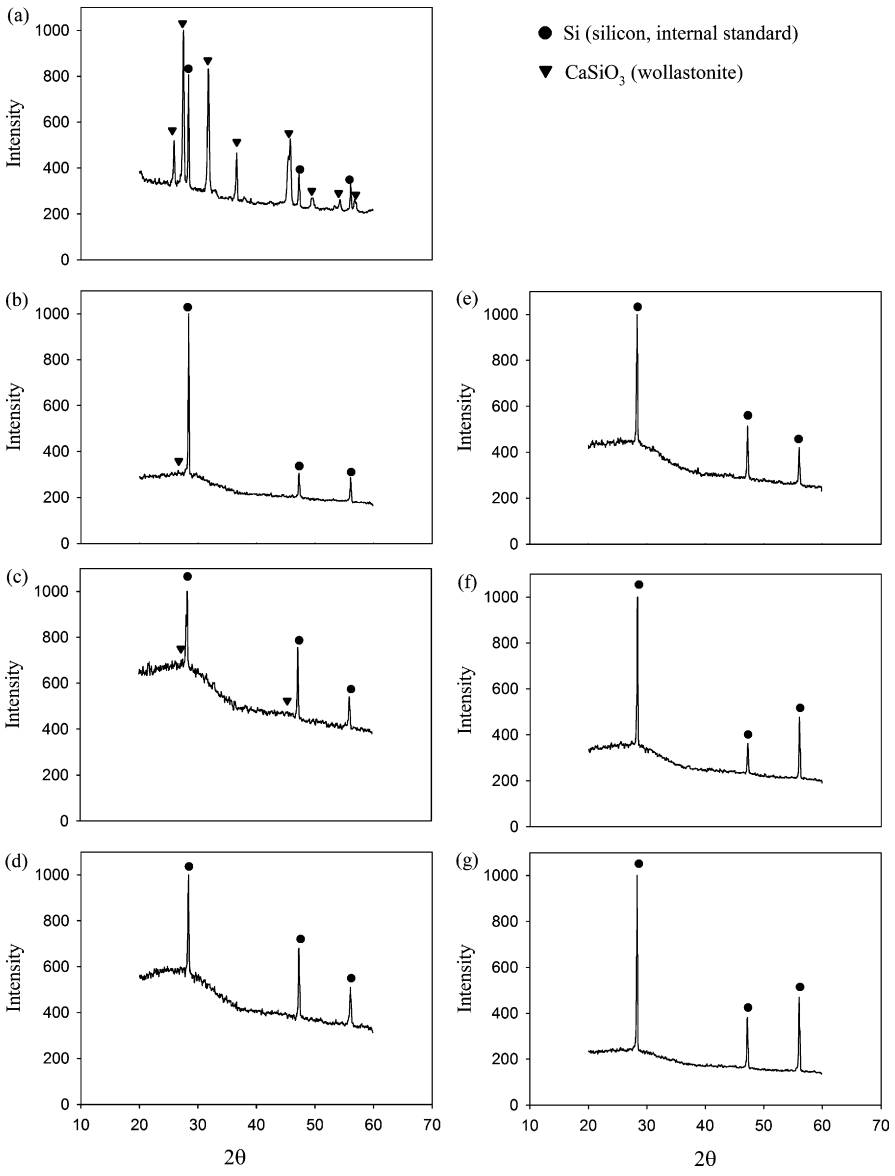

Fig. 2. XRD patterns of water-quenched slags: (a) W-0, (b) W-1, (c) W-2, (d) W-3, (e) W-4, (f) W-5, and (g) W-6.

were qualitatively examined and the leaching concentrations of slag metals were determined.

2. Experimental

2.1. Sample preparation and vitrification

To investigate the correlation between hazardous metal immobilization and glassy structure during vitrification, pure Al_2O_3, CaO, and SiO_2 served as glassy encapsulation phases and Cr, Cu, Mn, Ni, and Pb were referred to targeted hazardous metals. The targeted hazardous metal powders were doped in the forms $Cr(NO_3)_3{\cdot}9H_2O$, $Cu(NO_3)_2{\cdot}3H_2O$, $Mn(NO_3)_2{\cdot}4H_2O$, $Ni(NO_3)_2{\cdot}6H_2O$, and $Pb(NO_3)_2$ with the identical concentration of 1000 mg/kg (as metal ions). Table 1 shows physical properties of the targeted metals. The basicity (mass ratio of CaO to SiO_2) of 2/3 was used to obtain glass matrixes in vitrification [10]. The mole fractions of Al_2O_3 increased from S-0 to S-6 specimens (Table 2).

The specimens were vitrified using an electrical melting furnace with $MoSi_2$ alloy heating rods. The heating program was 50–1100 °C at 6 °C/min and 1100–1400 °C at 4 °C/min. After the thermal treatment, the samples were cooled by air without forced convection or using water quenching. The air-cooled and water-quenched slags were labeled with the prefixes of A and W, respectively, as shown in Table 3.

2.2. Compositions and metal leaching of slags

The vitrified slags were dried at 105 °C for 3 h, weighed, pulverized, and ground to grains that passed the mesh of a #200 sieve (smaller than 74 μm). Samples (0.5 g) were digested with mixed acids (5 mL of nitric acid [HNO_3] + 10 mL of perchloric acid [$HClO_4$] + 1 mL of fluoroboric acid [HBF_4]) in Teflon vessels in a microwave digester. The heating program was 25–180 °C at 10 °C/min, held isothermally for 15 min, and then cooled to room temperature. The digests were diluted to 25 mL with deionized water, filtered by a cellulose ester filter with a pore size of 0.8 μm, and analyzed using atomic absorption spectroscopy (AAS, SensAA, GBC).

To evaluate the recyclable application of slags, the toxicity characteristic leaching procedure (TCLP) was performed to estimate the mobility of hazardous metal species. The procedures of extraction,

Table 4
Variation of slag structure versus mole fraction of Al ion.

Specimen	Stage I	Stage II		Stage III		Stage IV	
	A-0	A-1	A-2	A-3	A-4	A-5	A-6
Al mol%	0		>0–15	15–25		>25	
AVF (%)	25.7		40–50	>90		78.6	46.5
NBO/T of the glass matrix	1.43	1.22	0.99	0.74	0.45	0.12	0
Predominate crystalline phase	$CaSiO_3$	$CaSiO_3$		None		$CaAl_2Si_2O_8$	
NBO/T of the crystalline phase	2	2		–		0	
Category of crystalline phase	Inosilicate	Inosilicate		–		Tectosilicate	
Role of Al ions	–	Intermediate		Intermediate and network former		Network former	

NBO/T: nonbridging oxygens to tetrahedrally coordinated cations ratio.

digestion, dilution, and filtration all followed USEPA Method 1311 [15]. The concentrations of metal species in TCLP extracts and solid digests, including Al, Cr, Cu, Mn, Ni, and Pb, were measured using AAS to determine the leaching concentrations of metals and the compositions of slags for calculating the percent mass retained (PMR = (mass retained in slag/mass in original specimen) × 100%) of metals.

2.3. Crystalline characteristics and microstructures

X-ray diffraction (XRD) analysis was utilized to determine the crystalline phases in slags. In all cases, samples were ground to <74 μm fine powders. A powder diffractometer (Geigerflex 3063) with Ni-filtered CuK_α radiation was used for the measurement. The detector scanned over a range of 2θ angles from 20° to 60° at a step size of 0.01° and a dwell time of 0.15 s per step. Crystalline phases of specimens were identified by comparing the intensities and positions of peaks in XRD spectrums with those listed in the Joint Committee on Powder Diffraction Standards (JCPDS) data files.

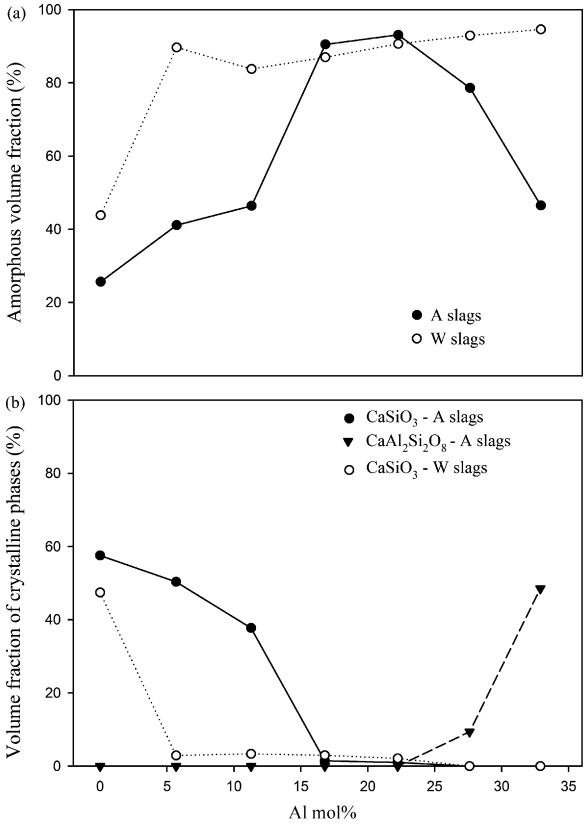

Fig. 3. Volume fractions of (a) amorphous and (b) crystalline phases in air-cooled (A) and water-quenched (W) slags.

In this study, the volume fractions of crystalline phases in slags were also measured according to XRD analysis using internal standard addition [16]. The internal standard, high-purity silica crystal powders, was added with a Si/sample mass ratio of 0.1; it served as a reference material in the crystalline semi-quantitative analysis. The approximate volume fraction of the crystalline phase was then determined by comparing the areas of specific peaks with that of internal standard. The detailed procedure was given in a previous report [17]. The amorphous volume fractions (AVFs) of slags were calculated using the following equation:

$$\mathrm{AVF} = 1 - \sum_{i=1}^{n} \mathrm{CP}_i$$

CP_i: the volume fraction of the ith crystalline phase.

The microstructures of slags were qualitatively examined using scanning electron microscopy–energy dispersive spectroscopy (JEOL JXA-840 SEM–EDS). Powdery samples with particle sizes smaller than 74 μm were stuck on a metallic plate, coated with a film of Au using an ion sputter coater, and then scanned by SEM.

3. Results and discussion

3.1. Compositions of slags

Table 3 shows composition and percent mass retained data of the targeted metals in slags. The profiles of metals in all slags were similar; thus, A-0 and W-0 were used to represent other slags. The

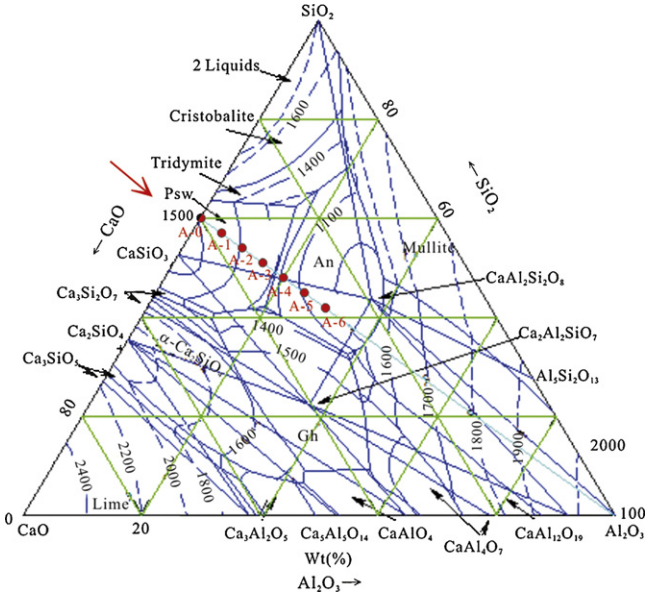

Fig. 4. Phase diagram of $CaO–Al_2O_3–SiO_2$ ternary system.

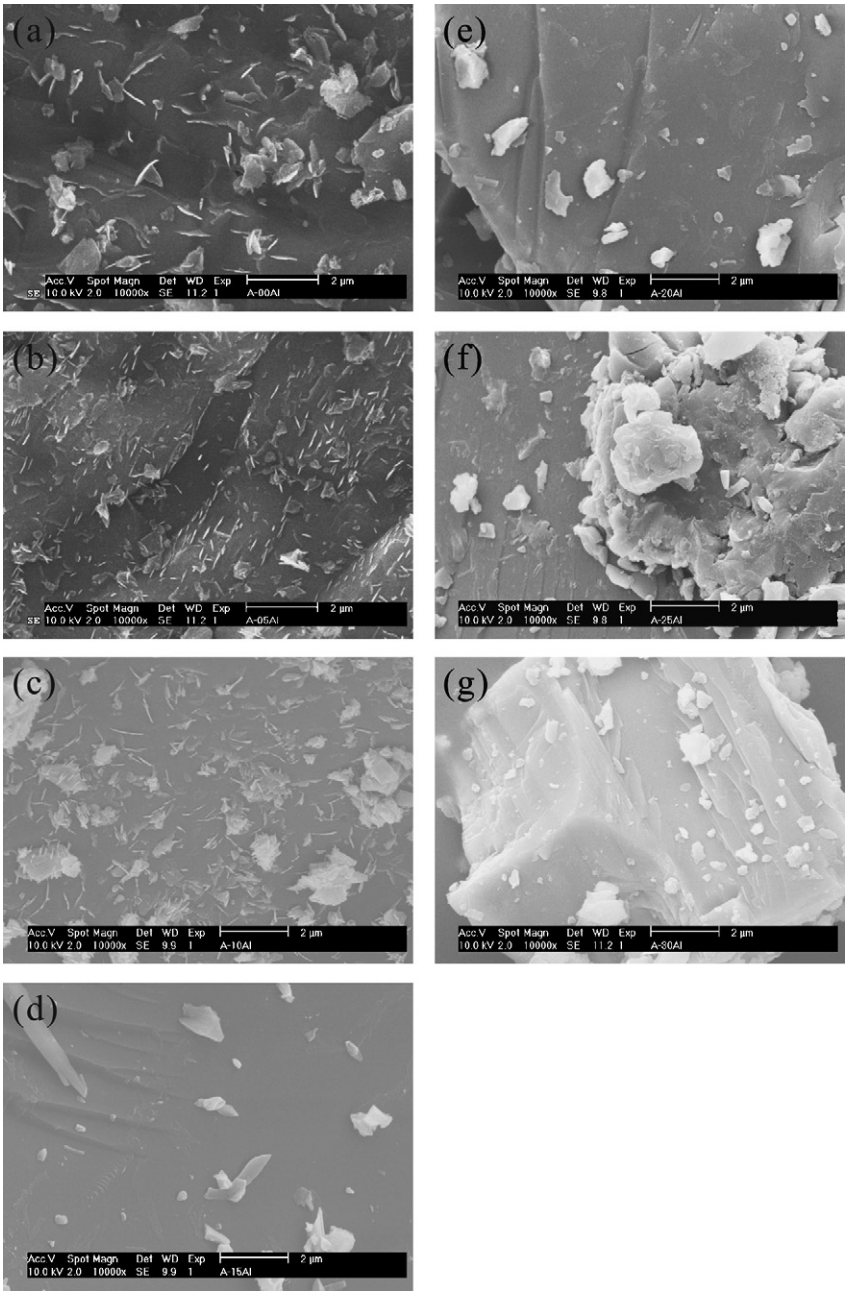

Fig. 5. SEM images of air-cooled slags: (a) A-0, (b) A-1, (c) A-2, (d) A-3, (e) A-4, (f) A-5, and (g) A-6.

content of Cr, Cu, Mn, Ni, and Pb was 1240, 855, 1450, 1130, and 178 mg/kg, respectively in air-cooled slags and was 1020, 517, 1270, 809, and 197 mg/kg, respectively in water-quenched slags. Compared to the metal content in samples before vitrification, most of Cr, Cu, Mn, and Ni was retained in slags but most Pb was vaporized after vitrification. The PMR values of Cr, Cu, Mn, and Ni in slags ranged from 0.521 to 1.44, but that of Pb was below 0.2. A previous study reported that PMR values of metal species which tended to remain in slags commonly ranged from 0.5 to 2 [18]. The discrepancy between input mass and output mass of each targeted metal was probably due to sampling error caused by the heterogeneous distribution of metals among specimens.

3.2. Crystalline characteristics of slags

The XRD patterns with marked crystalline phases of air-cooled and water-quenched slags are shown in Figs. 1 and 2, respectively. The volume fractions of the crystalline and amorphous phases were measured by semi-quantitative XRD analysis (Fig. 3). For water-quenched slags, only W-0 had a significant crystalline phase of $CaSiO_3$, wollastonite (47.5%). No noteworthy crystalline phases were found in other slags. For air-cooled slags, A-0 had notable crystalline phases of SiO_2, quartz (10.4%) and $CaSiO_3$ (57.6%), but the crystalline phase of SiO_2 was not present in slags containing Al ions. With an increase of Al mol%, the volume fraction of crystalline $CaSiO_3$ decreased and it reached zero in the Al mol% range of 15–25%. At higher Al mol%, Al ions were incorporated to form a new crystalline phase, $CaAl_2Si_2O_8$ (anorthite), with crystalline volume fractions of 9.37% and 48.5% in A-5 and A-6, respectively.

The AVFs of the water-quenched slags (except for W-0) were all greater than 80%, indicating that the water quenching greatly enhanced formation of amorphous structure when Al ions existed. In contrast, the AVFs of air-cooled slags ranged from 20% to 40% at Al mol% < 15%, and were greater than 90% at Al mol% within 15–25%.

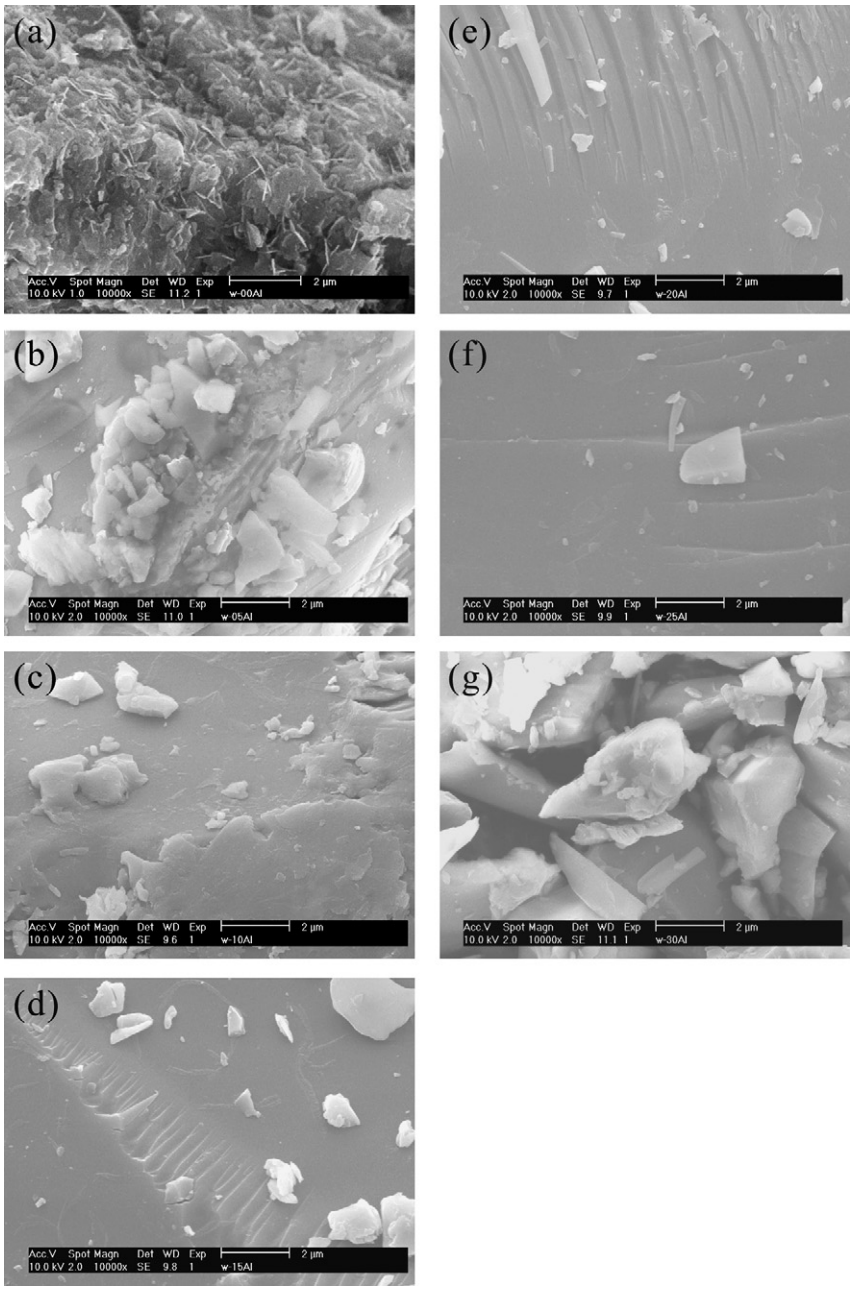

Fig. 6. SEM images of water-quenched slags: (a) W-0, (b) W-1, (c) W-2, (d) W-3, (e) W-4, (f) W-5, and (g) W-6.

However, the AVFs approached 46.5% at Al mol% higher than 30%. This phenomenon indicates that air-cooled slags were vitrified to form glassy amorphous matrixes in a limited range of Al mol%.

3.3. Variation of crystalline structure versus Al mol%

Using the water quenching treatment, all slags except for W-0 exhibited amorphous structures, indicating that Al ions are essential for the formation of amorphous glassy matrixes. However, there was no significant difference in crystalline volume fraction among the water-quenched slags with various Al mol%. Therefore, we examined the structures of air-cooled slags to determine the role of Al during vitrification. A SiO_4 tetrahedron of silicate glass with 4 surrounding oxygen atoms that are commonly classified as bridging or nonbridging depending on whether they are shared between neighboring tetrahedra or not. The ratio of nonbridging oxygens to tetrahedrally coordinated cations (NBO/T) usually serves as an index that reflects the extent of polymerization of a silicate melt. The NBO/T ratio ranges from 0 (a fully polymerized melt) to 4 (a fully depolymerized melt consisting of an isolated tetrahedron). According to the crystalline characteristics, the variation of air-cooled slag structure can be divided into four stages (Table 4) that are stated as follows.

1. *Stage I*. Without any Al ion addtion in this stage, the structure was highly crystallized (AVF = 25.7%) and the major crystalline phase of A-0 was $CaSiO_3$ which is a simple chain structure (inosilicate). For a glass matrix with a high NBO/T value (1.43), SiO_4 tetrahedra only linked into chains by sharing two of the four oxygen atoms, but the chains were independent of each other.
2. *Stage II*. With Al mol% less than 15%, the NBO/T value decreased to around unity. In this stage, Al ions served as an intermediate

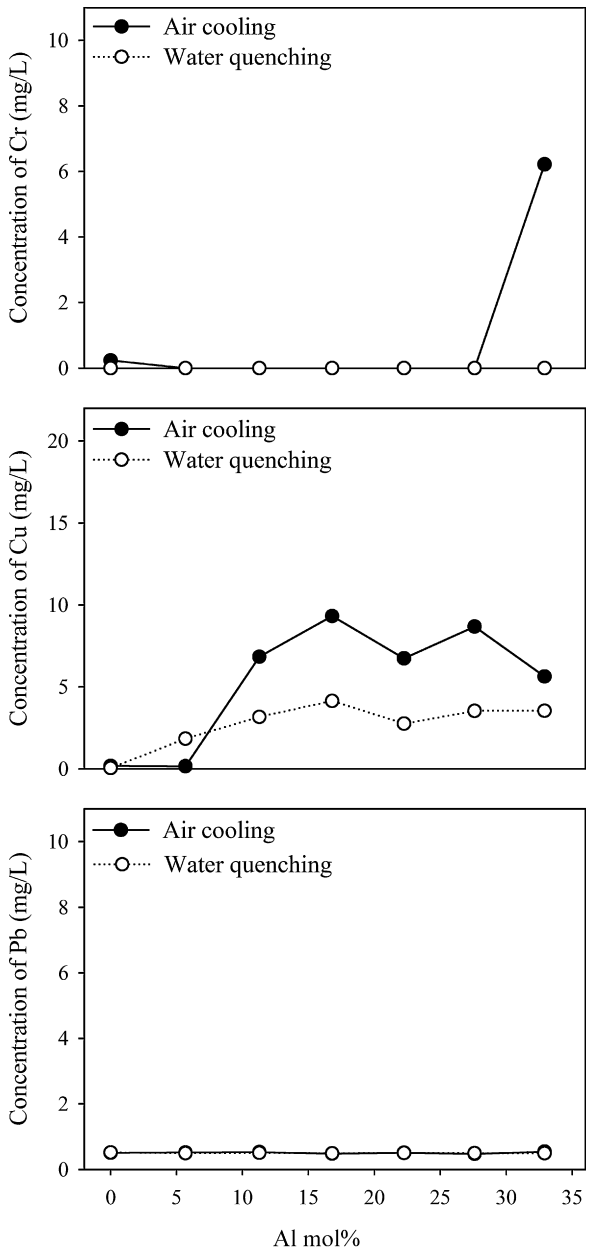

Fig. 7. Concentrations of regulated metals in TCLP extracts of slags.

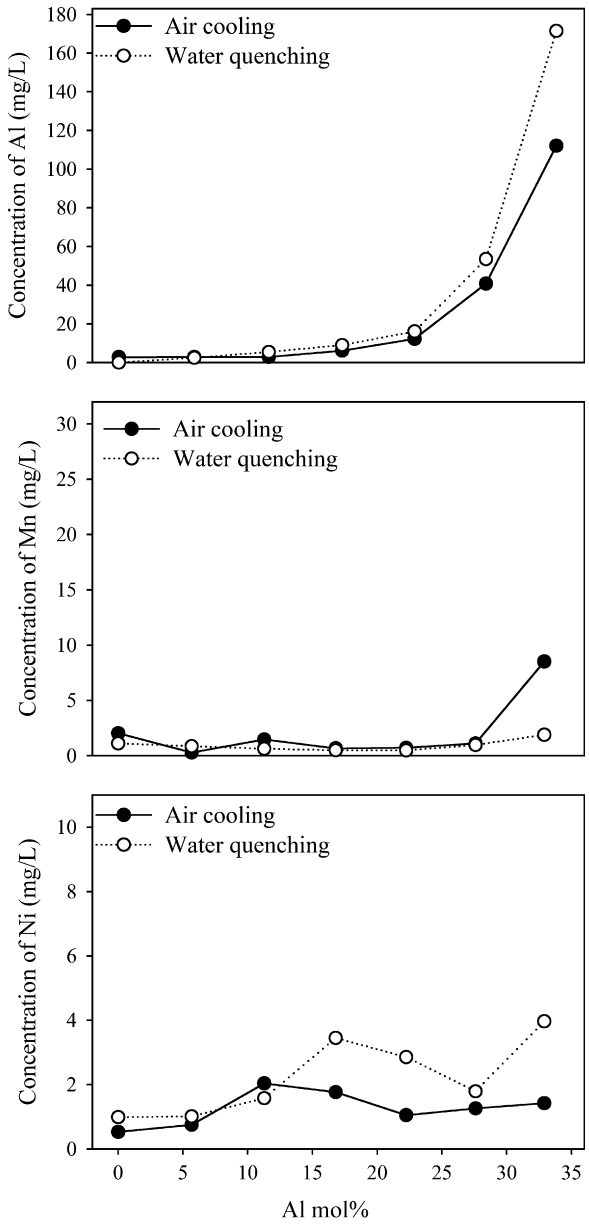

Fig. 8. Concentrations of unregulated metals in TCLP extracts of slags.

that initially linked one tetrahedron chain to another; they were also incorporated into the crystalline phase. However, the linked chains were disordered so the volume fraction of $CaSiO_3$ in this stage decreased as the Al mol% increased.

3. *Stage III*. In stage III, the AVFs of slags were higher than 90%, indicating that the slag structure transformed from crystalline into glassy amorphous ones. The increase of Al ions decreased NBO/T to around 0.5, and thus the slag structure was highly polymerized. In this stage, Al ions acted both as an intermediate and a network former; therefore, they not only linked the chains of silicates but also replaced the Si atoms in the glassy frame. Therefore, the atomic arrangement was highly disordered, resulting in the formation of amorphous structure.
4. *Stage IV*. When Al mol% was higher than 25%, a new crystalline phase ($CaAl_2Si_2O_8$, a tectosilicate) was formed. This crystalline phase is a three-dimensional frame of linked SiO_4 tetrahedra, revealing that the structure was highly polymerized with the aid of Al ions. For A-5, the NBO/T value was 0.12, indicating that oxygen atoms were highly bridged in the glass matrix. At higher Al mol%, the theoretical NBO/T of A-6 was −0.25 according to the mole ratio of the glass matrix. However, it is impossible to have a negative NBO/T ratio so the value was taken as 0. This finding implies that there was an excess amount of Al_2O_3 for the polymerization of the structure, and some Al ions were not incorporated into but isolated from the glass matrix.

There are two reasons for why Al ions can replace Si ions in the formation of minerals. One is that the sizes of these two ions are approximately equal and the other is that they have the same oxygen coordinate number when Al ions act as a glass former instead of an intermediate. For the latter phenomenon, two Si^{4+} ions (per feldspar unit) in the Si_4O_8 framework are substituted by two Al^{3+} ions and the electrostatic charge of the network is balanced by one Ca^{2+} ion [12]:

$$Si_4O_8\text{framework} + 2Al^{3+} + Ca^{2+} \rightarrow CaAl_2Si_2O_8 + 2Si^{4+}$$

In this reaction, Al ions replace Si ions as the center of the tetrahedron and transform the SiO_4 tetrahedron into an AlO_4 one. The Al ions connect additional nonbridging oxygen ions and convert them into bridging ones, thus causing the decrease of NBO/T ratio [11]. Such connections may link with SiO_4 tetrahedra in polymerized grouping. The ordered bridging and high degree of polymerization resulted in a crystallized structure with high amount of $CaAl_2Si_2O_8$ in A-6. On the W-6 side, the water quenching process made the arrangement disordered and the structure amorphous.

Fig. 4 marks the positions of A-0 to A-6 in order along an arrow on the phase diagram of a $CaO–Al_2O_3–SiO_2$ ternary system. For Stages I and II, A-0, A-1, and A-2 were located in the $CaSiO_3$ formation region which matched the identification of $CaSiO_3$ in slags of these specimens. As the Al mol% increased, the locations of A-3 and A-4 moved to the fringe of the $CaSiO_3$ and $CaAl_2Si_2O_8$ formation regions; thus, the formation of a crystalline phase was not attributed to either $CaSiO_3$ or $CaAl_2Si_2O_8$, and an amorphous structure was formed. Points A-5 and A-6 were in the $CaAl_2Si_2O_8$ formation region, which explains why $CaAl_2Si_2O_8$ was formed and why the fraction increased for such two air-cooled slags. The crystalline phases in slags determined by XRD analysis also support the locations of crystalline phase formation regions in the $CaO–Al_2O_3–SiO_2$ ternary phase diagram.

3.4. Microstructures of slags

Figs. 5 and 6 show the SEM images of air-cooled and water-quenched slags, respectively. A-0, A-1, and A-2 (Fig. 5a, b, and c, respectively) exhibited acicular crystalline structures that agree with the shape of $CaSiO_3$. For A-3 and A-4 (Fig. 5d and e, respectively), amorphous structure formed and no noticeable crystal was found on the surface. When Al mol% increased to ≥25% (Fig. 5f and g), crystalline structures appeared and bulk aggregation was observed.

For water-quenched slags, Fig. 6a shows that W-0 had many crystals with a shape similar to that of A-0. According to the XRD analysis, the major crystalline phases in the two slags were identical but they had different crystalline fractions. With the addition of Al_2O_3, the fraction of crystalline phase drastically decreased and instead an amorphous structure formed. This phenomenon was also seen in other water-quenched slags. For W-2 to W-5 (Fig. 6c–f, respectively), amorphous structures with small fractions of crystalline phases were observed. However, at a higher Al mol%, W-6 (Fig. 6g) turned into small pieces with glassy sharp-edged agglomeration.

Comparing the SEM images of air-cooled and water-quenched slags, the major crystalline phases of A-0 and W-0 were both $CaSiO_3$ with morphological similarity. In the Al mol% range between 5% and 15%, the acicular crystalline structure was observed in air-cooled slags but it was not present in water-quenched slags. When the Al mol% values were 15–25%, air-cooled and water-quenched slags were both amorphous. For the A-5/W-5 and A-6/W-6 pairs, the structures of W-5 and W-6 were amorphous, but A-5 and A-6 exhibited noticeable crystalline characteristics that were significantly different from those of water-quenched slags. Overall, the SEM observations agreed with the results of XRD analysis.

3.5. Leaching tests of toxic metals in slags

Figs. 7 and 8 show the leaching concentrations of some regulated and unregulated metals (in slags), respectively, based on the toxicity characteristic leaching procedure [19]. The Cr concentrations in TCLP extracts were near zero, except for A-6. There are two possible reasons. First, the high Cr leaching concentration was probably due to more leachable Cr from more intensive surface oxidation in an air cooling environment. Second, the A-6 had a highly crystallized structure which is less capable of encapsulating metals. The Cu leaching concentrations of air-cooled slags were slightly higher than those of water-quenched ones. These results were similar to those reported in an earlier work [20].

However, the variation of Al mol% did not affect the leaching concentration of Cu. The leaching concentrations of Pb in slags were all close to 0.5 mg/L. According to their PMR data, most of Pb was vaporized during vitrification and the little Pb left in slags was due to encapsulation regardless of the structure or Al mol% of slags.

The trends of Al leaching concentration versus Al mol% were similar for air-cooled and water-quenched slags. When the Al mol% increased to 20%, the leaching concentration of Al significantly increased, indicating that excess Al_2O_3 probably existed in soluble forms instead of being incorporated into the glass matrix. The TCLP concentrations of Mn ranged from 0.5 to 2 mg/L but the leached Mn was higher in A-6 (8.5 mg/L). This phenomenon is similar to that for Cr. It can be explained by slag surface oxidation that may promote the formation of highly soluble Mn. Therefore, the highly crystallized structure of A-6 is not suitable for immobilizing metals in slags.

4. Conclusions

The role of Al in the formation of slags was investigated using semi-quantitative XRD analysis and SEM. In a non-Al environment, the crystalline phase of $CaSiO_3$ was formed in both air-cooled and water-quenched slags. With the addition of Al_2O_3, no crystalline phase was observed in water-quenched slags. For air-cooled slags, Al ions initially acted as an intermediate that linked one tetrahedron chain to another, reducing the amount of crystalline phase with the Al mol% in the range of 5–15%. At 15–25 Al mol%, the increase of the linking effect turned the slags into an amorphous structure. At >25 Al mol%, the Al ions acted as network formers only and replaced Si ions in the network. The ordered arrangement and substitution in the silicate framework made the structure of A-6 highly crystallized. The variation of crystalline phase versus Al mol% matched that of $CaO–Al_2O_3–SiO_2$ ternary phase diagram. According to XRD and TCLP analyses, the air cooling enhanced the formation of crystallize structures while the metal leaching was relatively higher in such structures.

References

[1] Y.M. Kuo, J.W. Wang, C.H. Tsai, Encapsulation behaviors of metals in slags containing various amorphous volume fractions, J. Air Waste Manage. 57 (2007) 820–827.
[2] C.T. Li, W.J. Lee, K.L. Huang, S.F. Fu, Y.C. Lai, Vitrification of chromium electroplating sludge, Environ. Sci. Technol. 41 (2007) 2950–2956.
[3] L.S. Pioro, B.F. Sadovskiy, I.L. Pioro, Research and development of a high-efficiency one-stage melting converter-burial-bunker method for vitrification of high-level radioactive wastes, Nucl. Eng. Des. 205 (2001) 133–144.
[4] Y.M. Kuo, T.C. Lin, P.J. Tsai, W.J. Lee, H.Y. Lin, Fate of polycyclic aromatic hydrocarbons during vitrification of incinerator ash in a coke bed furnace, Chemosphere 51 (2003) 313–319.
[5] Y.M. Kuo, T.C. Lin, P.J. Tsai, Metal behavior during vitrification of incinerator ash in a coke bed furnace, J. Hazard. Mater. B109 (2004) 79–84.
[6] K. Park, J. Hyun, S. Maken, S. Jang, J.W. Park, Vitrification of municipal solid waste incinerator fly ash using Brown's gas, Energy Fuels 19 (2005) 258–262.
[7] K. Kakimoto, Y. Nakano, T. Yamasaki, K. Shimizu, T. Idemitsu, Use of fine-grained shredder dust as a cement admixture after a melting, rapid-cooling and pulverizing process, Appl. Energy 79 (2004) 425–442.
[8] E. Bernardo, M. Varrasso, F. Cadamuro, S. Hreglich, Vitrification of wastes and preparation of chemically stable sintered glass–ceramic products, J. Non-Cryst. Solids 352 (2006) 4017–4023.
[9] C.T. Li, Y.J. Huang, K.L. Huang, W.J. Lee, Characterization of slags and ingots from the vitrification of municipal solid waste incineration ashes, Ind. Chem. Eng. Res. 42 (2003) 2306–2313.
[10] Y.M. Kuo, T.C. Lin, P.J. Tsai, Effect of SiO_2 on immobilization of metals and encapsulation of a glass network in slag, J. Air Waste Manage. 53 (2003) 1412–1416.
[11] W.D. Kingery, H.K. Bowen, D.R. Uhlmann, Introduction to Ceramics, 2nd ed., John Wiley & Son, Inc., New York, 1976.

[12] J.D. Dana, in: C. Klein (Ed.), The Manual of Mineral Science, 22nd ed., John Wiley & Son, Inc., New York, 2002.
[13] K.L. Lin, K.S. Wang, B.Y. Tzeng, N.F. Wang, C.Y. Lin, Effects of Al_2O_3 on the hydration activity of municipal solid waste incinerator fly ash slag, Cement Concr. Res. 34 (2004) 587–592.
[14] F. Peng, K. Liang, A. Hu, H. Shao, Nano-crystal glass-ceramics obtained by crystallization of vitrified coal fly ash, Fuel 83 (2004) 1973–1977.
[15] Environmental Protection Administration of United Stated Toxicity Characteristic Leaching Procedure: SW846 Method 1311.
[16] B.D. Cullity, S.R. Stock, Elements of X-ray Diffraction, 3rd ed., Prentice Hall, Upper Saddle River, 2001.
[17] C.Y. Chen, G.S. Lan, W.H. Tuan, Preparation of mullite by the reaction sintering of kaolinite and alumina, J. Eur. Ceram. Soc. 20 (2000) 2519–2525.
[18] L.L. Oden, W.K. Connor, ASME/US vitrification of residue (ash) from municipal waste combustion systems Bureau of Mines Investigation Program Report on 1994, 24, ASME Research Committee on Industrial and Municipal Wastes Subcommittee on Ash Vitrification, 1994, pp. 71–101.
[19] Environmental Protection Administration, Executive Yuan, Taiwan, Standards for Defining Hazardous Waste, 2006.
[20] Y.M. Kuo, J.W. Wang, H.R. Chao, C.T. Wang, G.P. Chang-Chien, Effect of cooling rate and basicity during vitrification of fly ash: Part 2. On the chemical stability and acid resistance of slags, J. Hazard. Mater. 152 (2008) 554–562.